J Mater Sci (2017) 52:1823–1830

Needle-disk electrospinning inspired by natural point discharge

Zhi Liu[1], Koon Keong Jeremy Ang[3], and Jihuan He[1,2,*]

[1] National Engineering Laboratory for Modern Silk, College of Textile and Clothing Engineering, Soochow University, 199 Ren-Ai Road, Suzhou 215123, China
[2] Nantong Textile Institute, Soochow University, Nantong, China
[3] School of Civil and Environmental Engineering, Nanyang Technological University, Singapore 639798, Singapore

Received: 18 May 2016
Accepted: 4 October 2016
Published online: 13 October 2016

ABSTRACT

Point discharge is a natural phenomenon which principle and application are both under active investigation. In this work, a needle-disk electrode spinneret was designed through the combination of the point discharge concept and the merits of typical needleless electrospinning (disk as spinneret). The desired outcome for point electrode system is to produce a controllable process of jet formation, with respect to the control of jet site and amount of jets under a lower applied voltage value. Two comparisons were used: (i) in comparison to the typical needleless electrospinning method (disk electrospinning), the needle-disk electrospinning produce finer and more uniform nanofibers. Further numerical simulation results confirmed that the needle-disk electrode induced electric field intensity which is 5.33 times higher than that of disk electrode under the same parameters; (ii) both the numerical simulation and experimental results showed that needle-disk electrospinning can produce competitive quality of nanofibers accompanied by enhanced throughput, compared with the traditional single-needle electrospinning method. Finally, we demonstrate that needle-disk electrospinning produces nanofiber with super-high throughput of 13.5 g/h, which is 183 times higher than traditional electrospinning under similar spinning conditions.

Introduction

In recent decades, electrospinning technique evokes high interest owing to its facile capacity to manufacture nanofibers with numerous remarkable properties [1, 2].

However, the typical low production rate plagues traditional single-needle electrospinning (TNE) for further application of nano-materials. To improve the productivity, frontier researches focus on multi-needle electrospinning positioning needles with special geometrical structure [3–5]. Although multi-needle electrospinning reasonably enhanced the productivity, it

Address correspondence to E-mail: hejihuan@suda.edu.cn

DOI 10.1007/s10853-016-0472-9

however brings significant drawbacks including jet to jet interferences, high cost, and nozzle clogging [6]. These lead researchers towards simultaneously triggering multiple polymeric jets from a free liquid surface to increase productivity, to industrialize the level of production. Lukas et al. [7] has explained a generalized mechanism of multiple jets from free liquid surface. When the applied electric field intensity is above a critical value, waves of an electrically conductive liquid self-organize on a microscopic scale, and finally form jets originating from the wave crests. This mechanism was proved by Miloh et al. [8] who investigated electrical instability and multiple jets from a spherical liquid layer. Results show that the liquid layer becomes wavy due to the action of electric field. This subsequently creates wave crests which begin to grow and finally evolve into multiple polymeric jets at critical voltage value. Therefore, the jet formation process is unstable and uncontrollable due to the uncertain site of jet formation and a different size of the protuberant Taylor-like cone, resulting in a wide distribution of fiber diameter. Additionally, smooth liquid surface on previous spinneret means a uniform electrical field distribution [9]. As a result, much stronger electrical field is required atop the liquid surface, for the formation of wave crests to then generate multiple polymeric jets [10]. On one hand, needleless electrospinning such as disk electrode [11], wire electrode [12, 13], cylinder electrode [14], magnet auxiliary electrode [15], plate edge electrode [16], bowl edge electrode [17], cone electrode [18], and cleft electrode [19] pose a smooth surface on spinneret. On the other hand, the phenomenon of point discharge in which electrical field intensively concentrates on the object bulge is analogous to how protuberant objects in nature are normally strike by lightning. The principle of point discharge has drawn great attention both in fundamental research [20] and practical application such as plasma reactions [21, 22] and ozone generation [23, 24]. In these applications, a self-sustained and electrical discharge takes place in the vicinity of an electrode at a low voltage supply.

Therefore, point electrode may provide the solution to mass production of nanofiber at low applied voltage value. Figure 1 shows the numerical simulation results of the electric field around the point electrode at various angles (from the plane view of the needle tip). The results are calculated using Maxwell 2D program (ANSOFT Corporation). It is noteworthy that many previous researches applied the numerical simulation method by Maxwell program to evaluate the electrical field intensity and distribution of electrospinning apparatus [17, 25]. As shown in Fig. 1, the electrical field strongly concentrates on electrode tip and reaches the maximum point at the vertex. The three different angles presented in Fig. 1. show an electrical field intensity of 8.34×10^6 V/m of 109° (Fig. 1a), 9.85×10^6 V/m of 18° (Fig. 1b) and 1.51×10^7 V/m of 6° (Fig. 1c), indicating that the curvature of the point electrode significantly affects the electrical field intensity.

From these observations, we designed a needle-disk electrode with multiple point electrodes. In our previous study, our design has shown to be capable of fabricating a variety of polymers similar to TNE [26]. In this work, we focus on (i) the spinning process with respect to the polymeric liquid entrainment, jet formation, jet stretch, and nanofiber solidification;

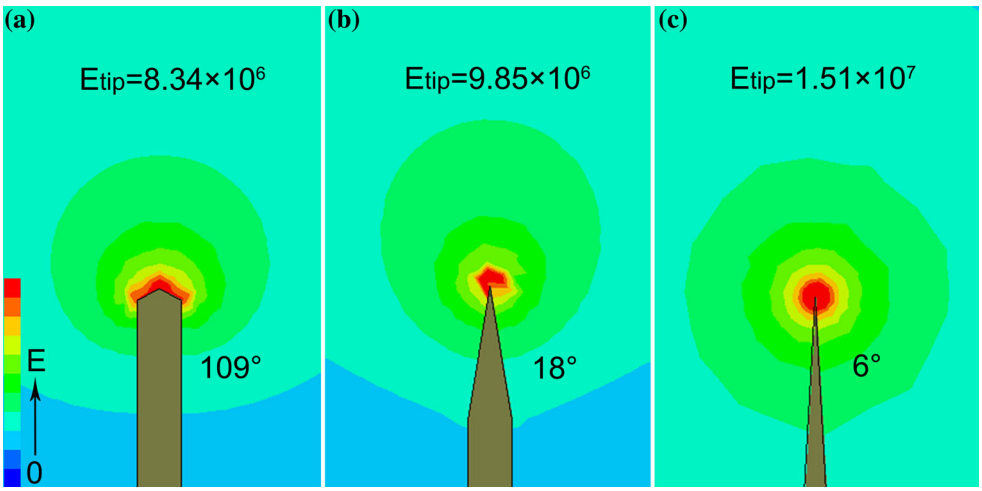

Figure 1 Numerical simulation of single point electrode with different electrode curvatures. The electrode length is 8 mm and the diameter is 0.8 mm. The voltage value in the simulation process is 25 kV.

(ii) the comparison with typical needleless electrospinning (disk electrospinning); and (iii) the comparison with TNE, with regard to the nanofiber quality and throughput.

Experimental

Materials

Poly(vinylidene fluoride-*co*-hexa-fluoropropylene) (PVDF-HFP, M_w 400,000) was purchased from Aladdin Industrial Corporation, Shanghai, China. *N*,*N*-dimethyl formamide and acetone were supplied by Sinopharm Chemical Reagent Co., Ltd. (Suzhou, China). All reagents were analytical grade and were used as received without further treatment.

Preparation of PVDF-HFP nanofiber by three typical spinning methods

PVDF-HFP was dissolved in binary solvent of *N*,*N*-dimethyl formamide/acetone (weight ratio of 5:5) at room temperature, to obtain a 12 wt% solution. The applied voltage of disk electrospinning is 35 kV while needle-disk electrospinning and TNE is 25 kV. The collection distances of three electrospinning methods are the same (25 cm). The rotation rate of disk electrospinning and needle-disk electrospinning was chosen as 25 rpm, and the flow rate of TNE maintained as 0.8 ml/h. The ambient relative humidity and temperature used in the spinning process were 50 ± 2 % and 25 ± 2 °C, respectively, and kept constant.

Measurement and characterization

The morphology of electrospun PVDF-HFP nanofibers was observed using an SEM (Hitachi S-4800, Tokyo, Japan) at 20 °C, 60 RH. Samples were sputter-coated with gold layer prior to imaging. The diameters of PVDF-HFP fibers were calculated by measuring at least 100 fibers at random using *Image J* program. Optical images were photographed by a digital camera (SONY, α35, Japan).

The electric field around the electrode was calculated using Maxwell 2D (ANSOFT Corporation). The Maxwell program utilizes finite element methods and adaptive meshing to achieve a converged solution. In the simulation process, the calculation finished at energy error and delta energy less than 1 %. The excitation voltage is 25 kV for three electrodes. Particularly, for TNE, the protuberant angle of polymer liquid was based on the Taylor cone 49.3°; for needle-disk electrode, the thickness of polymer liquid on needle surface was set as 0.1 mm based on [8].

Nanofiber productivity was measured using weight method. Firstly, the resulting membrane (spinning for 1 h) heated at 60° for 6 h to remove the residual solvent. Then, three pieces each with an area of 1.5×1.5 cm^2 (named as $\text{Area}_{\text{piece}}$) were tailored from the membrane at different locations. The average weight of the three pieces was recorded as $\text{weight}_{\text{piece}}$. Subsequently, the total area of the membrane was measured, named as $\text{Area}_{\text{total}}$. Then, the productivity can be obtained using the following equation:

$$\text{Productivity}(\text{g/h}) = \text{weight}_{\text{piece}} \times (\text{Area}_{\text{total}}/\text{Area}_{\text{piece}})$$

Results and discussion

The spinning process of needle-disk electrospinning

We formulated four steps for the formation of nanofiber for one needle in Fig. 2a: (i) the lower part of needle-disk is immersed into the polymer solution, and as the needle-disk rotates through the polymeric liquid, the polymer liquid was entrained on the surface of the needle. As the needle-disk travels away from the polymeric solution, the entrained liquid flows towards the needle bottom due to gravitational force, while surface tension and viscous force resist such procedure, synergistically developing a thinning liquid film coating on the needle surface; (ii) with applied potential, the external field deforms the liquid film, leading to a difficultly visible droplet on needle tip. In this process, the redistribution of the positive and negative ions in the polymer fluid induces a finite electric field [27]. Such induced electric field modifies the original electrical field resulting from applied potential. When the coupled electrical field intensity reaches a threshold, the jet initiates from the droplet tip where the surface tension can no longer sustain the static equilibrium situation [28]; (iii) the electrically charged jet is stretched and thinned by the electrical force, and flows away from the needle tip for a few centimeters long in a nearly straight line. A conical shape (Fig. 2b) is then formed at the end of the straight segment

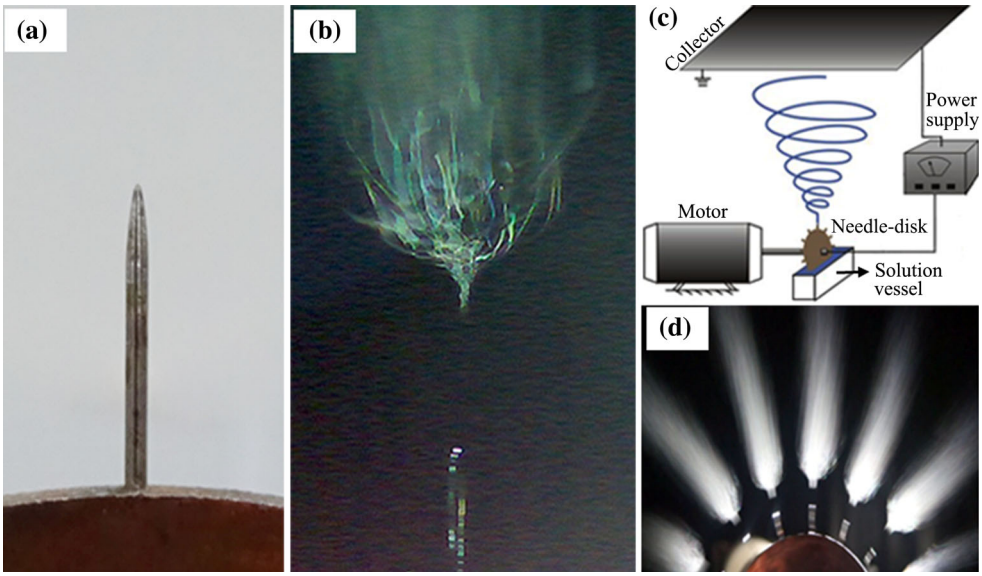

Figure 2 **a** Optical image of single needle used in our lab. It is note that the needle is not hollow, **b** jet with a conical shape photographed by a high-speed camera, **c** schematic of needle-disk electrospinning apparatus, and **d** optical image of multiple jets.

when the jet is so thin and fast that it cannot maintain the straight line condition; (iv) the jet subjected to blending instabilities driven by electricity [29], whipping in a complex path. This whipping further stretches and makes the jet thinner. Subsequently, nanofibers are deposited on the collector after solvent evaporation.

In the spinning process, the needle coated with polymeric liquid, indicative of wave crests, provide the active site of jet formation. The addition of the active sites enables controllable jet formation process. We further develop this spinning process of single needle to a multiple point electrode system shown in Fig. 2c containing a motor, a solution vessel, a needle-disk as spinneret, an aluminum plate as collector, and a high-voltage direct-current power supply. With the rotation of needle-disk, polymeric liquid entrains on the needle surface constantly. As anticipated, the setup of continuous multiple jets is demonstrated in Fig. 2d. Furthermore, from the special point electrode spinneret and spinning process, the jet number and nanofiber productivity can be conveniently tuned by adjusting the needle and disk number.

The comparison between the disk electrospinning and the needle-disk electrospinning

For the present model of needle-disk electrode Fig. 3, the needle length is 8 mm and needle diameter is 0.8 mm with 24 needles arranged in a needle-disk. The diameter and thickness of the needle-disk and disk electrode is the same, 96 and 2 mm, respectively. Figure 3 illustrates the comparison between the disk electrospinning and the needle-disk electrospinning. For disk electrospinning, the electrical field concentrates on disk edge with a low value of 1.26×10^6 V/m (Fig. 3a), which is consistent with previous study [30]. As a result, a high-voltage supply is needed to trigger the jet formation, typically larger than 40 kV. However, for needle-disk electrospinning, the electrical field is powerfully concentrated on needle tip with a value of 6.72×10^6 V/m (Fig. 3c), which is 5.33 times higher than that of disk electrospinning. The results of the experiment agree with the simulated calculations. As shown in Fig. 3b, the PVDF-HFP nanofibers fabricated by disk electrospinning show non-uniform morphology (diameter 463.24 ± 89.75 nm) with a wide diameter distribution from 122 to 741 nm (Fig. 4). Inversely, the needle-disk electrospinning can fabricate finer nanofiber (Fig. 3d) with average diameter of 245.23 ± 33.75 nm and uniform nanofiber with narrow diameter distribution from 181 to 357 nm (Fig. 4).

The comparison between the TNE and the needle-disk electrospinning

Previous needleless electrospinning enhances the nanofiber throughput at the cost of nanofiber quality such as bad fiber uniformity and higher fiber diameter. Therefore, the enhancement of nanofiber throughput while maintaining the quality of TNE fiber simultaneously is an ongoing challenge. The simulated results showed the induced electrical field

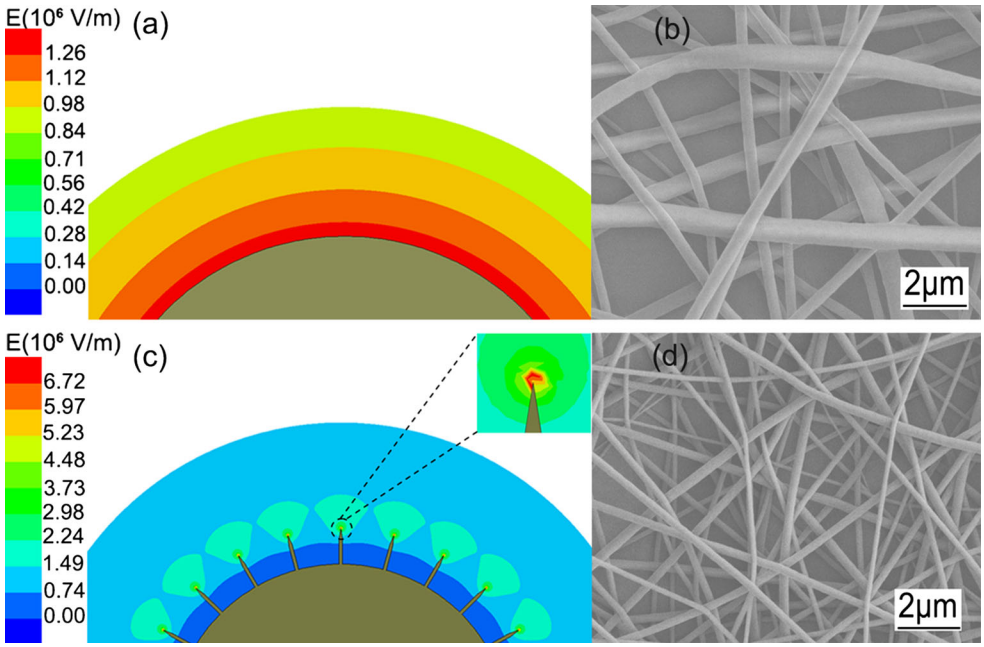

Figure 3 **a** Simulation result of electrical field of disk electrode, **b** PVDF-HFP nanofibers fabricated by disk electrospinning, **c** simulation result of electrical field of needle-disk electrode; the angles (from the plane view of the needle tip) of needle-disk is 20°, and **d** PVDF-HFP nanofibers fabricated by needle-disk electrospinning.

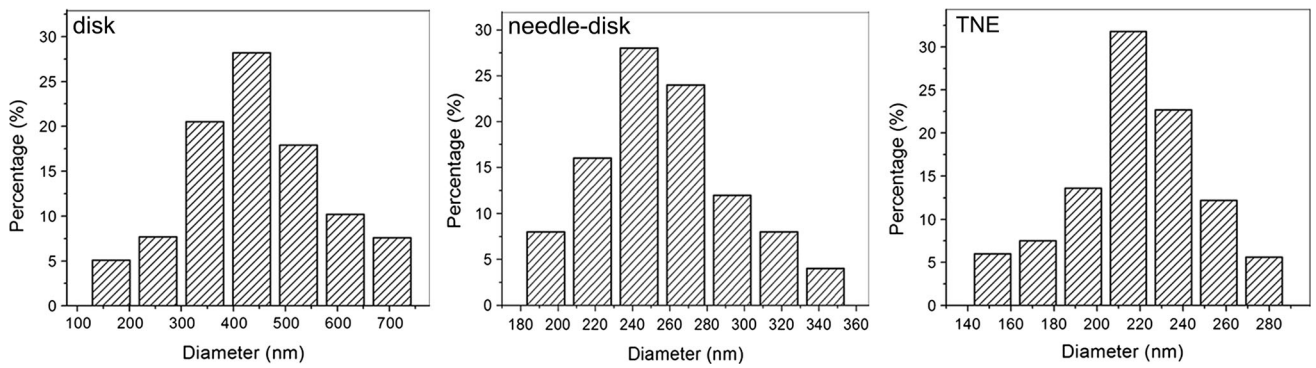

Figure 4 Diameter distribution of electrospun PVDF-HFP nanofibers fabricated by three typical electrospinning methods.

intensity 5.64×10^6 V/m of TNE, while 6.54×10^6 V/m of needle-disk electrode (Fig. 5a, b). And the resulting PVDF-HFP nanofiber by TNE (Fig. 5c) revealed a uniform morphology with diameter (226.63 ± 27.68 nm) and narrow diameter distribution (141–288 nm) (Fig. 4). As for the needle-disk electrospinning, the observed nanofiber diameter is 245.23 ± 33.75 nm and diameter distribution ranges from 181 to 357 nm (Fig. 4), suggesting that needle-disk electrospinning can fabricate high-quality nanofiber like TNE.

To evaluate the nanofiber productivity of the facile spinning method, the comparison between TNE and needle-disk electrospinning was carried out. As described in experimental section, the two methods were used to spin PVDF-HFP for 1 h under the same conditions. Using the weight method, the results were obtained and presented in Fig. 6. The overall nanofiber productivity of needle-disk electrospinning is 13.5 g/h, which is 183-folds higher than TNE. For comparison, nanofiber productivity of other method is listed in Table 1. Clearly, the cylinder spinneret [14], magnet auxiliary method [15], plate edge spinneret [16], bowl edge spinneret [17], and cleft spinneret [19] achieved a relatively lower nanofiber productivity.

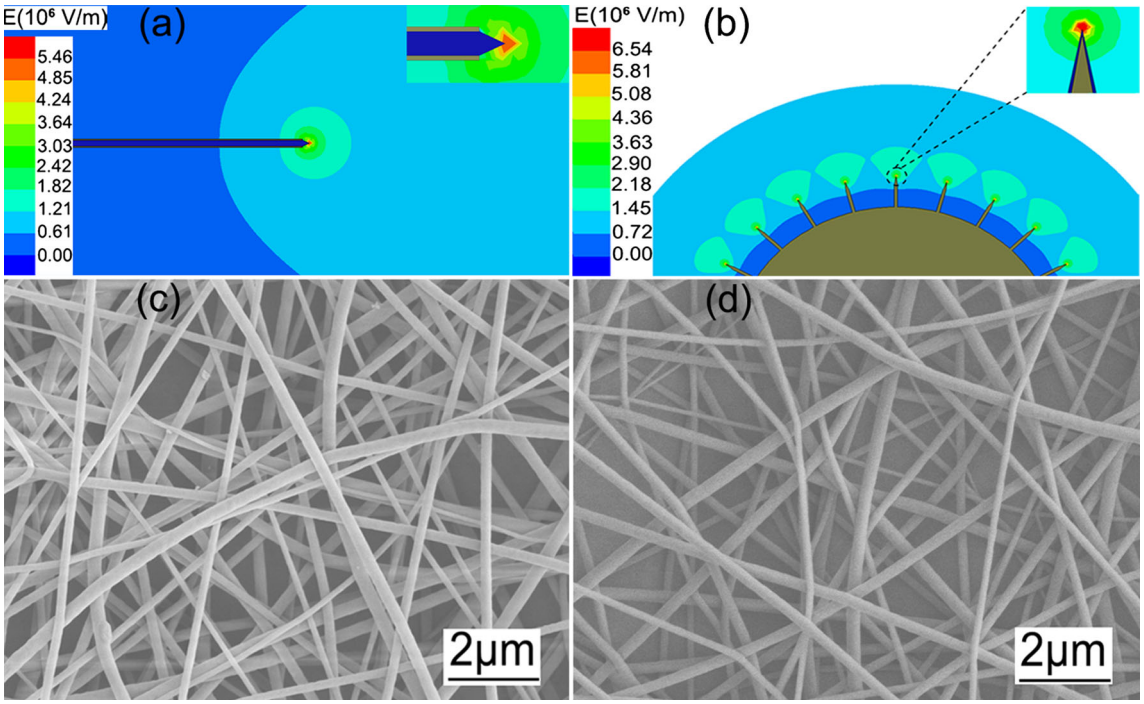

Figure 5 **a** Simulation result of electrical field of TNE electrode, **b** simulation result of electrical field of needle-disk electrode, **c** PVDF-HFP nanofibers fabricated by TNE, and **d** PVDF-HFP nanofibers fabricated by needle-disk electrospinning.

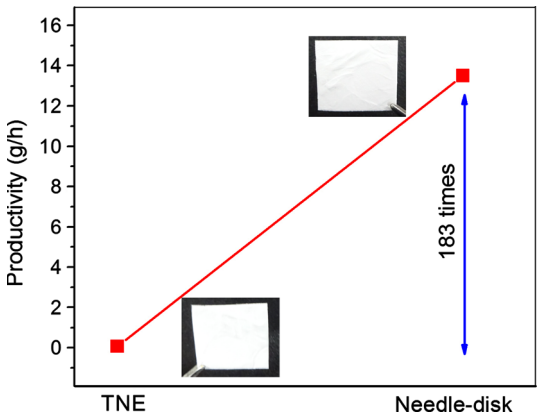

Figure 6 Nanofiber productivity of needle-disk electrospinning and TNE. The inserted figures are the optical images of PVDF-HFP membrane piece each with an area of 1.5 × 1.5 cm^2.

Table 1 Comparison of nanofiber productivity between needle-disk electrospinning and other spinning technology

Spinneret	Productivity	Voltage
Magnet auxiliary [15]	12 times than TNE	10^5 V/m
Cylinder [14]	25 times than TNE	40–50 kV
Bowl edge [17]	40 times than TNE	–
Porous tube [31]	250 times than TNE	20 kV
Twisted wire [12]	5.23 g/h	25–30 kV
Rotary cone [32]	10 g/min	30 kV
Wire electrode [25]	1 mg/min cm of electrode	35 kV
Plate edge [16]	10 times than TNE	28 kV
Cleft electrode [19]	7–16 ml/h	32–43 kV
Conical wire coil [18]	2.75 g/h	70 kV
Disk [30]	7.5 g/h	57 kV
Needle-disk	183 times than TNE	25 kV

Although porous tube [31] and rotary cone [32] spinneret possess high nanofiber productivity, they show a wide fiber diameter distribution. Likewise, conical wire coil [18] and disk spinneret [30] also observe high productivity rate, but a higher applied voltage is required in these spinning processes (Table 1). As for the twisted wire spinneret [11], the resulting nanofiber displayed dissimilar fiber diameter at different collector areas of the fiber, which will pose problems for application which requires fiber uniformity like membrane distillation [33]. Therefore, needle-disk electrospinning shows a good equilibrium between nanofiber quality and nanofiber throughput at a lower voltage supply.

Conclusions

In summary, point electrode was discussed based on the concept of point discharge, from which the single point electrode was further developed into a multiple point electrode system, the needle-disk electrospinning. This needle-disk electrospinning possesses two dominant merits: (i) having an active and controllable process of jet formation; (ii) inducing ultra-high electrical field intensity at the needle tip, allowing for the fabrication of nanofiber at a low applied voltage value. This multiple point electrode system is beneficial to fundamental research as well as practical application of nano-materials. Moreover, the needle-disk electrospinning method does require additional auxiliary energy to drive the spinneret, which should be a consideration in practical applications.

Acknowledgements

This work was supported by the Priority Academic Program Development of Jiangsu Higher Education Institutions (PAPD) and National Natural Science Foundation of China under Grant No. 11372205. We also like to acknowledge China Scholarship Council for the support and Dr. Darren Sun Delai for helpful remarks.

Compliance with ethical standards

Conflict of interest The authors declare that they have no conflict of interest.

References

[1] Liu C, Hsu PC, Lee HW, Ye M, Zheng G, Liu N, Li WY, Cui Y (2015) Transparent air filter for high-efficiency PM 2.5 capture. Nat Commun 6:6205. doi:10.1038/ncomms7205

[2] Sun Y, Wei Z, Zhang W, Li P, Lian K, Hu J (2016) Synthesis of brush-like ZnO nanowires and their enhanced gas-sensing properties. J Mater Sci 51:1428–1436. doi:10.1007/s10853-015-9462-6

[3] Theron SA, Yarin AL, Zussman E, Kroll E (2005) Multiple jets in electrospinning: experiment and modeling. Polymer 46:2889–2899

[4] Kim G, Cho YS, Kim WD (2006) Stability analysis for multi-jets electrospinning process modified with a cylindrical electrode. Eur Polym J 42:2031–2038

[5] Kumar A, Wei M, Barry C, Chen J, Mead J (2010) Controlling fiber repulsion in multijet electrospinning for higher throughput. Macromol Mater Eng 295:701–708

[6] Molnar K, Nagy ZK (2016) Corona-electrospinning: needleless method for high-throughput continuous nanofiber production. Eur Polym J 74:279–286

[7] Lukas D, Sarkar A, Pokorny P (2008) Self-organization of jets in electrospinning from free liquid surface: a generalized approach. J Appl Phys 103:084309. doi:10.1063/1.2907967

[8] Miloh T, Spivak B, Yarin AL (2009) Needleless electrospinning: electrically driven instability and multiple jetting from the free surface of a spherical liquid layer. J Appl Phys 106:114910. doi:10.1063/1.3264884

[9] Reznik SN, Yarin AL, Theron A, Zussman E (2004) Transient and steady shapes of droplets attached to a surface in a strong electric field. J Fluid Mech 516:349–377

[10] Kostakova E, Meszaros L, Gregr J (2009) Composite nanofibers produced by modified needleless electrospinning. Mater Lett 63:2419–2422

[11] Shuakat MN, Lin T (2015) Highly-twisted, continuous nanofiber yarns prepared by a hybrid needle-needleless electrospinning technique. RSC Adv 5:33930–33937

[12] Holopainen J, Penttinen T, Santala E, Ritala M (2014) Needleless electrospinning with twisted wire spinneret. Nanotechnology 26:025301. doi:10.1088/0957-4484/26/2/025301

[13] Bhattacharyya I, Molaro MC, Braatz RD, Rutledge GC (2016) Free surface electrospinning of aqueous polymer solutions from a wire electrode. Chem Eng J 289:203–211

[14] Tang S, Zeng Y, Wang X (2010) Splashing needleless electrospinning of nanofibers. Polym Eng Sci 50:2252–2257

[15] Yarin AL, Zussman E (2004) Upward needleless electrospinning of multiple nanofibers. Polymer 45:2977–2980

[16] Thoppey NM, Bochinski JR, Clarke LI, Gorga RE (2010) Unconfined fluid electrospun into high quality nanofibers from a plate edge. Polymer 51:4928–4936

[17] Thoppey NM, Bochinski JR, Clarke LI, Gorga RE (2011) Edge electrospinning for high throughput production of quality nanofibers. Nanotechnology 22:345301. doi:10.1088/0957-4484/22/34/345301

[18] Wang X, Niu H, Lin T, Wang X (2009) Needleless electrospinning of nanofibers with a conical wire coil. Polym Eng Sci 49:1582–1586

[19] Kula J, Linka A, Tunak M, Lukas D (2014) Image analysis of jet structure on electrospinning from free liquid surface. Appl Phys Lett 104:243114. doi:10.1063/1.4884597

[20] Gurevich AV, Karashtin AN (2013) Runaway breakdown and hydrometeors in lightning initiation. Phys Rev Lett 110:185005. doi:10.1103/PhysRevLett.110.185005

[21] Jiang B, Zheng J, Qiu S, Wu M, Zhang Q, Yan Z, Xue Q (2014) Review on electrical discharge plasma technology for wastewater remediation. Chem Eng J 236:348–368

[22] Eifert A, Petit J, Baier T, Bonaccurso E, Hardt S (2015) Inscribing wettability gradients onto polymer substrates with different stiffness using corona discharge in point-to-plane geometry. Appl Surf Sci 330:104–110

[23] Pasko VP (2003) Atmospheric physics: electric jets. Nature 423:927–929

[24] Pekárek S (2015) Effect of TiO_2 and reverse air supply on ozone production of negative corona discharge with the needle in the dielectric tube to mesh electrode system. Plasma Chem Plasma Process 35:705–719

[25] Forward KM, Rutledge GC (2012) Free surface electrospinning from a wire electrode. Chem Eng J 183:492–503

[26] Liu Z, Chen R, He J (2016) Active generation of multiple jets for producing nanofibers with high quality and high throughput. Mater Des 94:496–501

[27] Feng JJ (2002) The stretching of an electrified non-Newtonian jet: a model for electrospinning. Phys Fluids 14: 3912–3926

[28] Yarin AL, Koombhongse S, Reneker DH (2001) Taylor cone and jetting from liquid droplets in electrospinning of nanofibers. J Appl Phys 90:4836–4846

[29] Yarin AL, Koombhongse S, Reneker DH (2001) Bending instability in electrospinning of nanofibers. J Appl Phys 89:3018–3026

[30] Niu H, Lin T, Wang X (2009) Needleless electrospinning. I. A comparison of cylinder and disk nozzles. J Appl Polym Sci 114:3524–3530

[31] Dosunmu OO, Chase GG, Kataphinan W, Reneker DH (2006) Electrospinning of polymer nanofibers from multiple jets on a porous tubular surface. Nanotechnology 17:1123. doi:10.1088/0957-4484/17/4/046

[32] Lu B, Wang Y, Liu Y, Duan H, Zhou J, Zhang Z, Zhou J, Xie E (2010) Superhigh-throughput needleless electrospinning using a rotary cone as spinneret. Small 6:1612–1616

[33] Tijing LD, Choi JS, Lee S, Kim SH, Shon HK (2014) Recent progress of membrane distillation using electrospun nanofibrous membrane. J Membr Sci 453:435–462